18. Ruoff, A. L., Luo, H. & Vohra, Y. K. The closing diamond anvil optical window in multimegabar research. *J. Appl. Phys.* **69,** 6413–6416 (1991).
19. Inoue, K., Kanzaki, H. & Suga, S. Fundamental spectra of solid hydrogen. *Solid State Commun.* **30,** 627–629 (1979).
20. Van Straaten, J. & Silvera, I. F. Pressure dependence of the optical absorption edge of solid hydrogen in a diamond anvil cell. *Phys. Rev. B* **37,** 6478–6481 (1988).
21. Hemley, R. J., Hanfland, M. & Mao, H. K. High pressure dielectric measurements of solid hydrogen to 170 GPa. *Nature* **350,** 488–491 (1991).
22. Garcia, H. *et al.* Dielectric properties of solid molecular hydrogen at high pressure. *Phys. Rev. B* **45,** 9809–9715 (1992).
23. Dash, W. C. & Newman, R. Intrinsic optical absorption in single crystal germanium and silicon at 77° K and 300° K. *Phys. Rev.* **99,** 1151–1155 (1955).
24. Welber, B., Cardona, M., Kim, C. K. & Rodriguez, S. Dependence of the direct energy gap of GaAs on hydrostatic pressure. *Phys. Rev. B* **12,** 5729–5738 (1975).

Acknowledgements

We thank J. Eggert for interesting discussions and suggestions.

Competing interests statement

The authors declare that they have no competing financial interests.

Correspondence and requests for materials should be addressed to P.L. (e-mail: paul.loubeyre@cea.fr).

Outgassing from Amazonian rivers and wetlands as a large tropical source of atmospheric CO_2

Jeffrey E. Richey*, John M. Melack†, Anthony K. Aufdenkampe*, Victoria M. Ballester‡ & Laura L. Hess†

* *School of Oceanography, University of Washington, Seattle, Washington 98195, USA*
† *Institute for Computational Earth System Science, University of California, Santa Barbara, California 93106, USA*
‡ *Centro de Energia Nuclear na Agricultura, Caixa Postal 96, Piracicaba SP, Brazil*

Terrestrial ecosystems in the humid tropics play a potentially important but presently ambiguous role in the global carbon cycle. Whereas global estimates of atmospheric CO_2 exchange indicate that the tropics are near equilibrium or are a source with respect to carbon[1,2], ground-based estimates indicate that the amount of carbon that is being absorbed by mature rainforests is similar to or greater than that being released by tropical deforestation[3,4] (about 1.6 Gt C yr^{-1}). Estimates of the magnitude of carbon sequestration are uncertain, however, depending on whether they are derived from measurements of gas fluxes above forests[5,6] or of biomass accumulation in vegetation and soils[3,7]. It is also possible that methodological errors may overestimate rates of carbon uptake or that other loss processes have yet to be identified[3]. Here we demonstrate that outgassing (evasion) of CO_2 from rivers and wetlands of the central Amazon basin constitutes an important carbon loss process, equal to 1.2 ± 0.3 Mg C ha^{-1} yr^{-1}. This carbon probably originates from organic matter transported from upland and flooded forests, which is then respired and outgassed downstream. Extrapolated across the entire basin, this flux—at 0.5 Gt C yr^{-1}—is an order of magnitude greater than fluvial export of organic carbon to the ocean[8]. From these findings, we suggest that the overall carbon budget of rainforests, summed across terrestrial and aquatic environments, appears closer to being in balance than would be inferred from studies of uplands alone[3,5–6].

The major biogeochemical role of river systems in the global carbon cycle is typically considered to be the fluvial export of total organic carbon (TOC) and dissolved inorganic carbon (DIC) to the ocean (0.4–0.8 and 0.4 Gt C yr^{-1}, respectively)[9]. These fluxes are small components of the global C cycle, but they are significant compared to the net oceanic uptake of anthropogenic CO_2 (ref. 10). Aquatic carbon exports from terrestrial ecosystems, however, are not limited to fluvial discharge. Early measurements in the Amazon suggested that global CO_2 efflux (fluvial export plus respiration) from the world's rivers could be on the order of a gigatonne of carbon per year (Gt C yr^{-1}) (ref. 11). Recent measurements of mostly temperate rivers lead to estimates of global river-to-atmosphere fluxes of ~0.3 Gt C yr^{-1}, with evasion nearly equivalent to riverine TOC or DIC export[12]. Evasion from streams has been estimated to average 25–50% and 28–70% of the net annual carbon accumulation for tundra[13] and for peatlands[14], respectively. Hope *et al.*[14] cautioned that direct measurements of land–atmosphere CO_2 gas exchange that ignore water-borne fluxes might significantly overestimate terrestrial carbon accumulation.

The emphasis on export to the oceans and on individual streams does not, however, fully consider the spatial extent of a river network at regional scales. We evaluated the evasion of CO_2 from the fluvial environments of a 1.77 million km^2 quadrant of the low-gradient central Amazon basin (Fig. 1). Newly available remote sensing data sets for this quadrant have made it possible to quantify seasonal water coverage for representative low and high water periods. Combined with extensive measurements of dissolved CO_2 across the region we were able to compute the water-to-air fluxes of CO_2 for each environment.

We partitioned the quadrant into hydrographic environments—the Amazon mainstem channel, the mainstem floodplain, tributaries (channels and floodplains over 100 m in width, as constrained by the pixel dimensions of JERS-1 radar mosaics), and streams (channels and riparian zones less than 100 m in width). As computed from the radar mosaics, the flooded area of the mainstem and tributaries rose from 79,000 km^2 (about 4% of the quadrant area) in October 1995 to 290,000 km^2 (16% of the quadrant area) by May–June 1996. The low (21,000 km^2) and high water (51,000 km^2) areas estimated for streams were comparable to the area of the mainstem floodplain and greater than the area of the mainstem channel itself.

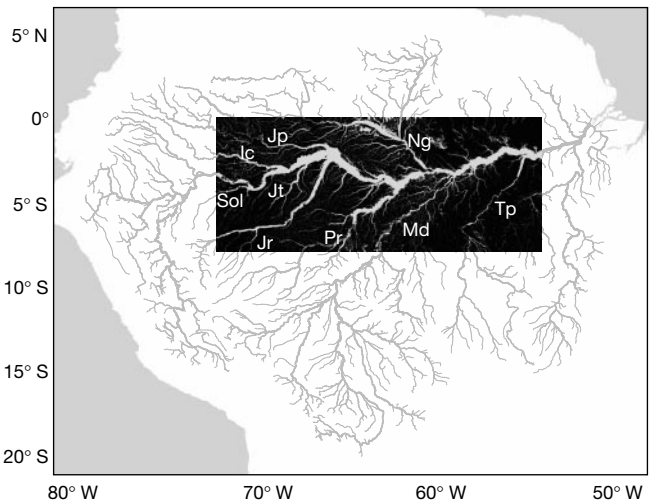

Figure 1 Flooded area of the central Amazon basin at high water, as mapped from the Japanese Earth Resources Satellite radar data (May–June 1996). The flooded area is shown as light areas in dark inset (the study quadrant). Underlying the inundation image is a digital river network (derived from the Digital Chart of the World, the GTOPO30 digital elevation model and ancillary cartographic information). Major tributaries are labelled: Negro (Ng), Japurá (Jp), Içá (Ic), Solimões (Sol, the Amazon mainstem exiting Peru), Jutaí (Jt), Juruá (Jr), Purus (Pr), Madeira (Md), and Tapajós (Tp).

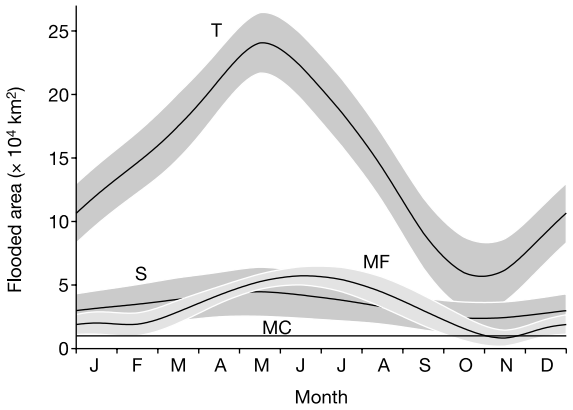

Figure 2 Spatially integrated annual sequences of surface water area for hydrographic environments as determined from JERS-1 radar data and multi-year hydrographic records. Hydrographic environments are divided into: the Amazon mainstem channel (MC); the mainstem floodplain (MF); the channels and floodplains of tributaries over 100 m wide (T); and the streams and riparian zones less than 100 m wide (S). Shaded regions represent 67% confidence intervals determined by Monte Carlo error propagation of both measurement uncertainties and interannual variability in river stage data.

Scaling to river stage height records and integrating over all sub-basins by hydrographic environment yielded the monthly extent of inundation for a typical year (Fig. 2). Tributaries south of the Amazon mainstem typically reached peak stage in April or May, whereas those to the north peaked in June or July. The result is that the region was most flooded in May (350,000 km^2 inundated, or 20% of the quadrant), with an annual mean flooded area of 250,000 km^2.

River and floodplain waters of the central Amazon basin maintain partial pressures of dissolved CO_2 (p_{CO_2}) that are supersaturated with respect to the atmosphere (Fig. 3). These concentrations track the hydrograph, increasing with rising water (to over 12,000 microatmospheres, μatm, in some tributaries) and decreasing with falling water. Average values over the year were 4,350 ± 1,900 μatm for all mainstem samples and 5,000 ± 3,300 μatm across the mouths of all major tributaries (compared to a mean of 3,200 μatm calculated for 47 large rivers from around the world[12]). The p_{CO_2} ranged from 2,950 μatm to over 44,000 μatm on the mainstem floodplain, averaging 14,100 ± 10,200 μatm upstream to 6,300 ± 4,200 μatm downstream.

High partial pressures of CO_2 translate to large gas evasion fluxes from water to atmosphere. By combining the areal extent of flooding and the distributions of p_{CO_2} with a simple but widely used gas evasion model, we observed a pronounced seasonality in evasion, corresponding to both the elevated water levels and the increased CO_2 concentrations (Fig. 4). Integrating over the year, the surface waters of the central Amazon basin (the 1.77 million km^2 quadrant) export 210 ± 60 Tg C yr^{-1} to the atmosphere. This corresponds to a flux of 8.3 ± 2.4 Mg C ha^{-1} yr^{-1} over the annual mean flooded area of the central basin, or 1.2 ± 0.3 Mg C ha^{-1} yr^{-1} over the entire quadrant.

Extrapolating across Amazonia, the total basin evasion is about 470 Tg C yr^{-1}. That is, the waters of the Amazon export about 13 times more carbon by CO_2 evasion to the atmosphere than by the export of total organic carbon (36 Tg C yr^{-1}) or of DIC (35 Tg C yr^{-1}) to the ocean[8]. Sub-basins within our study area exported 4 to 15 times more carbon by evasion than by discharge, suggesting that these findings may extend to other humid tropical river systems that drain weathered soils (and thus have low-alkalinity waters). These results are in contrast to findings from temperate river systems, where lower drainage density, higher-alkalinity waters and cooler temperatures lead to lower percentages of DIC being exported by evasion[12,15].

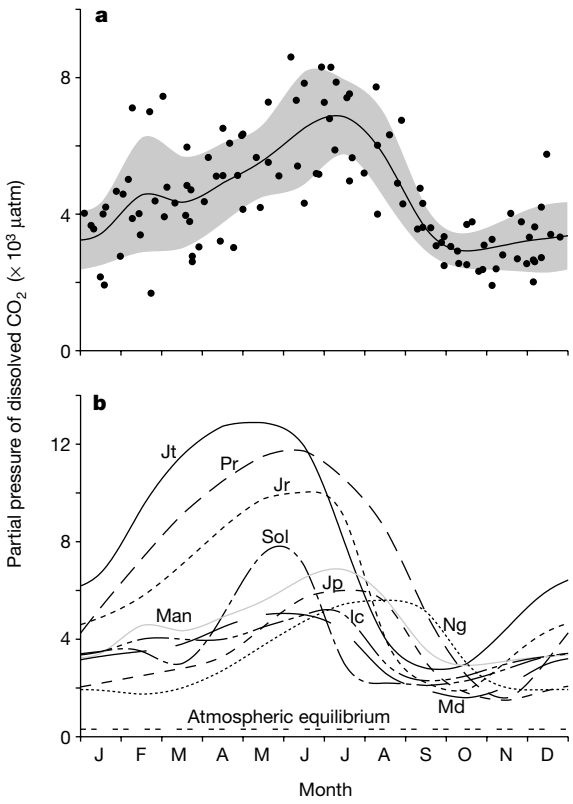

Figure 3 Seasonal distributions of carbon dioxide dissolved in rivers of the central Amazon basin. **a**, A ten-year time-series station on the mainstem Amazon near Manaus (Man, by the confluence of the Negro and Solimões) offers a high-resolution image of seasonality. **b**, Annual profiles for major tributaries derived from thirteen expeditions to observation stations at the mouth of each tributary (identified in Fig. 1) describe robust patterns of spatial heterogeneity.

The large evasion raises an important ecological question: what are the carbon sources that support such a flux? We evaluated potential terrestrial and aquatic sources of CO_2, both as CO_2 and as organic carbon that could be subsequently respired[16]. Although the following estimates have considerable uncertainty because of large temporal and spatial variability in the attributes of the respective environments, they do indicate the relative importance of the pathways leading to evasion. The partial pressure of CO_2 in the soil atmosphere is very high (15,000 μatm at the surface to 65,000 μatm with depth at forest and pasture sites in the eastern Amazon[17]), resulting from root respiration and the decomposition of organic matter. Dissolution of this CO_2 and its subsequent export to streams (using a typical water through-flow rate of 1.25 m yr^{-1}; ref. 18) is about 25% of the evasion. Dissolved organic carbon (DOC) concentrations in groundwater vary from 100 μM draining clay-rich oxisols to over 3,000 μM in groundwater draining sand-rich spodosols[19]. Assuming that oxisols predominate, groundwater DOC flux (computed as the product of the through-flow rate and DOC concentrations) is about 15% of the evasion. Litterfall, either directly into water or via entrainment by rising waters (estimated by applying litterfall rates for flooded forests[20] to the rivers and for upland forests[21] to the streams), is about 35% of the evasion. Root respiration and decomposition from floating and emergent macrophytes, which can fix atmospheric CO_2 directly and return some of that production to water, is about 25% of the evasion (computed from annual net production[20] and the area of habitat from a classification of the JERS-1 images). Organic matter and CO_2 derived from the algal (phytoplankton and periphyton) and submerged macrophyte production/respiration cycles are strictly aquatic, and thus cannot be considered as potential sources.

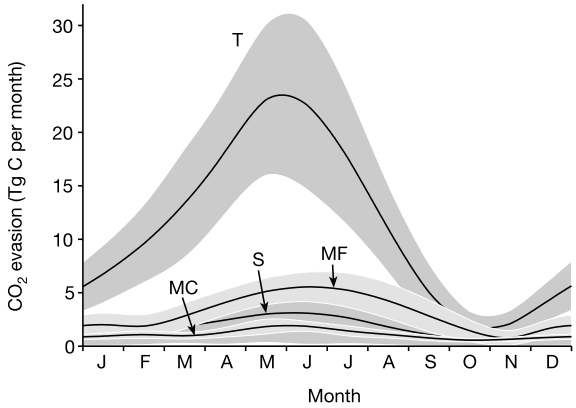

Figure 4 Spatially integrated sequences of monthly carbon dioxide evasion for the respective hydrographic environments (identified in Fig. 2). Lines represent the best estimate of long-term means, whereas shaded regions represent the 67% confidence interval for the range of values likely in a particular year. The upper confidence limit for streams, hidden from view, extends nearly to the upper limit for the mainstem floodplain.

In total, the estimate of carbon nominally available for evasion is consistent with the computed evasion. Of this amount, roughly 80% is of terrestrial upland and near-channel origin and about 20% is aquatic. Furthermore, approximately 75% originates as organic matter that would have to be respired in transit. This possibility is supported by previous work showing that DIC turnover time due to *in situ* respiration is 10–14 days for the large rivers of the Amazon[22]. Hence we hypothesize that evasion is driven primarily by in-stream respiration of organic carbon fixed originally on land and along river margins and mobilized into flowing waters. If true, linkages between land and water would be stronger than traditionally thought, with river corridors representing a significant downstream translocation of carbon originally fixed by the forest.

Assuming that the fluxes computed for the Amazon are representative of fluvial environments of lowland humid tropical forests in general, surface water CO_2 evasion in the tropics may help to explain an anomaly in the current balance of the global carbon cycle. Estimates that the tropics are a net carbon sink are not consistent with recent calculations from global inverse modelling, which imply that the tropics are at least in balance with the atmosphere if not a net source[1,2]. Extrapolating over the global area covered by humid tropical forests[3] with our estimate of areal evasion rates for the Amazon basin yields a flux of roughly $0.9\,\mathrm{Gt\,C\,yr^{-1}}$ (three times larger than previous estimates of global evasion[12]). A return flux from water to the atmosphere of this magnitude comes closer to reconciling independent carbon budgets for the tropics. □

Methods

Areal coverage of surface waters and flooding regime

Data from the Japanese Earth Resources Satellite-1 (JERS-1) L-band synthetic aperture radar were used to estimate the areal coverage and inundation status of rivers and floodplains over 100 m in width. Data were compiled into mosaics for periods of high water (May–June 1996) and low water (October 1995)[23]. For each mosaic, the study area was classified into either flooded or non-flooded areas based on radar backscatter intensities as delineated by image segmentation[24], and was divided into 25 tributary sub-basins from the river network (Fig. 1). The uncertainty of the procedure was estimated using high-resolution airborne, digital videography[25] to be ±5% at high water and ±10–15% at low water. To account for river corridors less than 100 m in width, we computed an area density function by extending a geometric series relating stream length and width to stream order from the river network for the whole basin (Fig. 1), and applied it to the study area. Mean monthly stage data from multiyear hydrographic records within each tributary sub-basin[18] were used to estimate tributary flooding sequences by assuming a temporal correspondence between stage height and areal extent of inundation. For five sub-basins without gauging records, the normalized hydrograph for the nearest neighbour with similar climatology was used. The temporal sequence of inundation within the mainstem and its floodplain was computed from multi-year monthly composite Scanning Multichannel Microwave Radiometer (SMMR) data[26].

CO_2 distributions

The seasonal and spatial distributions of p_{CO_2} within each hydrographic region were described from over 1,800 samples taken on 13 expeditions at different water stages throughout a 2,000 km reach of the central Amazon mainstem, tributary, and floodplain waters[8,22,27]. A ten-year time series[22] at the Marchantaria mainstem station gave a statistically robust picture of seasonal trends in p_{CO_2} (Fig. 3a). The standard deviation ranged from 16% to 37% of mean monthly values. Annual profiles for each tributary were similarly constructed, with assumed standard deviations of 40% for each month. For regions not directly sampled, profiles were used from the nearest neighbour with data, with assumed uncertainties of 80%. Floodplain measurements exhibited no obvious seasonal trends but a pronounced gradient from higher concentrations upriver to intermediate and then lower concentrations downriver. Hence we aggregated results by up-, mid-, and downriver sections.

Gas evasion

We computed evasion from the gas transfer model, $F = K(C_s - C_o)$, where F is the evasive flux, C_s is the surface water concentration, C_o is the atmospheric equilibrium, and K is the exchange coefficient. We determined K from direct measurements of O_2 and ^{222}Rn accumulation in free-floating chambers on the mainstem ($K = 2.3 \pm 0.9\,\mathrm{m\,d^{-1}}$) and primary tributaries ($K = 1.2 \pm 0.5\,\mathrm{m\,d^{-1}}$) and of CO_2 and CH_4 accumulation on the floodplain ($K = 0.65 \pm 0.25\,\mathrm{m\,d^{-1}}$)[28]. Chambers have been criticized on the basis that they may inhibit wind shear and alter the near-surface turbulence, but we assume that in the generally low wind environments of the Amazon and with the internal turbulence of large rivers of considerable flow velocity ($1–3\,\mathrm{m\,s^{-1}}$) this model yields a reasonable, if conservative, approximation of K. These values are comparable to values derived elsewhere not only with chambers but also with purposeful injections of inert gases, calculations with surface renewal models, and eddy covariance techniques[12,29,30].

To extrapolate to the entire Amazon basin (to compare to total fluvial export), we needed to estimate evasion for the 4.3 million km^2 of the Amazon basin outside our central quadrant, for which we do not have data. This region includes not only rainforest but also drier regions of savanna and Andean headwaters, and lacks the downstream extent of the large tributaries and mainstem. It includes, however, extensive wetlands of Bolivia and the northern and eastern Amazon, which could be large sources. We assumed, probably conservatively, that the areal evasion flux outside the quadrant is half that of inside.

Uncertainty analysis

Overall 67% confidence intervals of calculated values (given as ± standard error) were determined by Monte Carlo bootstrapping error propagation of both random measurement uncertainties and interannual variability of primary variables. Variability in stage height was simulated to show considerable covariation between hydrographic regions and also within a given year for a region, and variability in p_{CO_2} was set to covary to a lesser degree. All other variability was assumed to be spatially and temporally independent. Black lines in Figs 2, 3a and 4 are thus the best estimate of long-term means, whereas shaded regions represent the range in which values for an individual month might fall 67% of the time. Systematic differences in any chosen parameter, such as K, would proportionally shift our estimates of both means and confidence limits. As in any propagation of random uncertainty, integrated or summed values exhibit lower relative uncertainty than their individual components.

Received 31 August 2001; accepted 22 February 2002.

1. Schimel, D. S. *et al.* Recent patterns and mechanisms of carbon exchange by terrestrial ecosystems. *Nature* **414,** 169–172 (2001).
2. Gurney, K. R. *et al.* Towards robust regional estimates of CO_2 sources and sinks using atmospheric transport models. *Nature* **415,** 626–630 (2002).
3. Malhi, Y. & Grace, J. Tropical forests and atmospheric carbon dioxide. *Trends Ecol. Evol.* **15,** 332–337 (2000).
4. Houghton, R. A. A new estimate of global sources and sinks of carbon from land-use change. *Eos* **81,**(Suppl.), S281 (2000).
5. Grace, J. *et al.* Carbon dioxide uptake by an undisturbed tropical rain forest in Southwest Amazônia, 1992 to 1993. *Science* **270,** 778–780 (1995).
6. Malhi, Y. *et al.* Carbon dioxide transfer over a central Amazonian rain forest. *J. Geophys. Res.* **103,** 31593–31612 (1998).
7. Phillips, O. L. *et al.* Changes in the carbon balance of tropical forests: Evidence from long-term plots. *Science* **282,** 439–442 (1998).
8. Richey, J. E. *et al.* Biogeochemistry of carbon in the Amazon River. *Limnol. Oceanogr.* **35,** 352–371 (1990).
9. Degens, E. T., Kempe, S. & Richey, J. E. (eds) *Biogeochemistry of Major World Rivers* 323–397 (Wiley, Chichester, 1991).
10. Sarmiento, J. L. & Sundquist, E. T. Revised budget for the oceanic uptake of anthropogenic carbon dioxide. *Nature* **356,** 589–593 (1992).
11. Richey, J. E.,Brock, J. T., Naiman, R. J., Wissmar, R. C. & Stallard, R. F. Organic carbon: oxidation and transport in the Amazon River. *Science* **207,** 1348–1351 (1980).
12. Cole, J. J. & Caraco, N. F. Carbon in catchments: Connecting terrestrial carbon losses with aquatic metabolism. *Mar. Freshwat. Res.* **52,** 101–110 (2001).
13. Kling, G. W., Kipphut, G. W. & Miller, M. C. Arctic lakes and streams and gas conduits to the atmosphere: implications for tundra carbon budgets. *Science* **251,** 298–301 (1991).
14. Hope, D., Palmer, S. M., Billett, M. F. & Dawson, J. J. Carbon dioxide and methane evasion from a temperate peatland stream. *Limnol. Oceanogr.* **46,** 847–857 (2001).
15. Telmer, K. & Veizer, J. Carbon fluxes, pCO_2 and substrate weathering in a large northern river basin, Canada: carbon isotope perspectives. *Chem. Geol.* **159,** 61–86 (1999).
16. McClain, M. E. & Richey, J. E. Regional-scale linkages of terrestrial and lotic ecosystems in the Amazon basin: A conceptual model for organic matter. *Arch. Hydrobiol.* **113,** (Suppl.), 111–125 (1996).

17. Davidson, E. A. & Trumbore, S. E. Gas diffusivity and production of CO_2 in deep soils of the eastern Amazon. *Tellus B* **47,** 550–565 (1995).
18. Richey, J. E., Victoria, R. L., Mayorga, E., Martinelli, L. A. & Meade, R. H. in *Biospheric Feedbacks in Climate and the Hydrological Cycle* (ed. Kabat, P.) (Springer, in the press).
19. McClain, M. E., Richey, J. E., Brandes, J. A. & Pimentel, T. P. Dissolved organic matter and terrestrial-lotic linkages in the central Amazon Basin, Brazil. *Glob. Biogeochem. Cycles* **11,** 295–311 (1997).
20. Melack, J. M. & Forsberg, B. R. in *The Biogeochemistry of the Amazon Basin* (eds McClain, M. E., Victoria, R. L. & Richey, J. E.) 235–274 (Oxford Univ. Press, New York, 2001).
21. Chambers, J. Q., dos Santons, J., Ribeiro, R. J. & Higuichi, N. Tree damage, allometric relationships, and above-ground net primary production in central Amazon forest. *Forest Ecol. Management* **5348,** 1–12 (2000).
22. Devol, A. H., Forsberg, B. R., Richey, J. E. & Pimentel, T. P. Seasonal variation in chemical distributions in the Amazon (Solimões) River: a multiyear time series. *Glob. Biogeochem. Cycles* **9,** 307–328 (1995).
23. Siqueira, P. *et al.* A continental-scale mosaic of the Amazon Basin using JERS-1 SAR. *IEEE Trans. Geosci. Remote Sensing* **38,** 2638–2644 (2000).
24. Barbosa, C., Hess, L., Melack, J. & Novo, E. Mapping Amazon Basin wetlands through region-growing segmentation and segmented-based classification of JERS-1 data. *IX Latin Am. Symp. Remote Sensing (6–10 November 2000)* 1168–1176 (Universidad Nacional de Lujan, Puerto Iguazu, Argentina, 2000); see also ⟨http://www.selper.org⟩.
25. Hess, L. L. *et al.* Geocoded digital videography for validation of land cover mapping in the Amazon Basin. *Int. J. Remote Sensing* (in the press).
26. Sippel, S. J., Hamilton, S. K., Melack, J. M. & Novo, E. M. Passive microwave observations of inundation area and the area/stage relation in the Amazon River floodplain. *Int. J. Remote Sensing* **19,** 3055–3074 (1998).
27. Richey, J. E., Devol, A. H., Wofsy, S. C., Victoria, R. & Ribeiro, M. N. G. Biogenic gases and the oxidation and reduction of carbon in the Amazon River and floodplain waters. *Limnol. Oceanogr.* **33,** 551–561 (1988).
28. Devol, A. H., Quay, P. D., Richey, J. E. & Martinelli, L. A. The role of gas exchange in the inorganic carbon, oxygen and 222 radon budgets of the Amazon River. *Limnol. Oceanogr.* **32,** 235–248 (1987).
29. Clark, J. F., Wanninkhof, R., Schlosser, P. & Simpson, H. J. Gas exchange rates in the tidal Hudson River using a dual tracer technique. *Tellus B* **46,** 264–285 (1994).
30. MacIntyre, S., Eugster, W. & Kling, G. W. in *Gas Transfer at Water Surfaces* (eds Donelan, M. A., Drennan, W. M., Saltzman, E. S. & Wanninkhof, R.) 135–139 (American Geophysical Union, Washington, 2001).

Acknowledgements

We thank E. Mayorga, S. Denning, M. Gastil, D. Montgomery, R. Victoria, A. Krusche, A. Devol, P. Quay and J. Hedges for technical assistance and discussions, B. Forsberg and T. Pimental for fieldwork, and the Global Rain Forest Mapping Project of the National Space Development Agency of Japan for providing the JERS-1 radar data. This work was supported by the US NSF and NASA EOS and LBA projects, and by the Brazilian FAPESP programme.

Competing interests statement

The authors declare that they have no competing financial interests.

Correspondence and requests for materials should be addressed to J.E.R. (e-mail: jrichey@u.washington.edu).

Small-scale structure of the geodynamo inferred from Oersted and Magsat satellite data

Gauthier Hulot*, Céline Eymin*, Benoît Langlais*, Mioara Mandea* & Nils Olsen†

** Département de Géomagnétisme et Paléomagnétisme, CNRS UMR 7577, Institut de Physique du Globe de Paris, 4 Place Jussieu, B89, Tour 24, 75252 Paris cedex 05, France*
† Center for Planetary Science, Danish Space Research Institute, Julianes Maries Vej 30, DK-2100 Copenhagen, Denmark

The 'geodynamo' in the Earth's liquid outer core produces a magnetic field that dominates the large and medium length scales of the magnetic field observed at the Earth's surface[1,2]. Here we use data from the currently operating Danish Oersted[3] satellite, and from the US Magsat[2] satellite that operated in 1979/80, to identify and interpret variations in the magnetic field over the past 20 years, down to length scales previously inaccessible. Projected down to the surface of the Earth's core, we found these variations to be small below the Pacific Ocean, and large at polar latitudes and in a region centred below southern Africa. The flow pattern at the surface of the core that we calculate to account for these changes is characterized by a westward flow concentrated in retrograde polar vortices and an asymmetric ring where prograde vortices are correlated with highs (and retrograde vortices with lows) in the historical (400-year average) magnetic field[4,5]. This pattern is analogous to those seen in a large class of numerical dynamo simulations[6], except for its longitudinal asymmetry. If this asymmetric state was reached often in the past, it might account for several persistent patterns observed in the palaeomagnetic field[7–10]. We postulate that it might also be a state in which the geodynamo operates before reversing.

Thanks to the recent launch of the Danish Oersted satellite[3] (inclination 96.5°, altitude 638–849 km), 20 years after the 1979/80 US Magsat[2] analogous mission (97°, 325–550 km), two data sets at two different epochs are now available that can be used to construct high-degree spherical harmonic models of the geomagnetic field. (Degree 1 is the dipole field; the larger the degree, the smaller the length scale.) Taking advantage of this opportunity and relying on models[11] well suited for that purpose, we compute and investigate the changes that have occurred in the geomagnetic field between 1980 and 2000, focusing on the large to medium scales (that is, up to

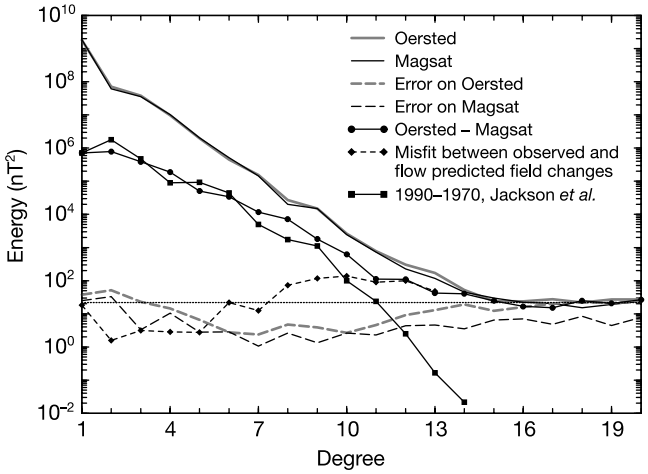

Figure 1 Spectra of the Oersted and Magsat models[11], of their error, of their difference, and of how well flows predict this difference. The spectrum of a model is constructed by plotting the contribution of each degree n of the spherical harmonic expansion to the average $\langle \mathbf{B}^2 \rangle$ of the predicted field **B** over the Earth's surface[1,2]. Errors in the Oersted and Magsat models are computed by analysing differences between models based on various data subsets[11]. Note the well-known[2] knee within the Oersted and Magsat spectra, showing that the main field probably dominates the signal for degrees less than 13, whereas the crustal field dominates for degrees larger than 15. A similar knee is seen around degree 15, in the Oersted–Magsat spectrum of the difference between the Oersted and Magsat fields. This knee, and the flat section of the spectrum beyond it, reveals disagreements between the high-degree signal sensed by Oersted and Magsat at a level slightly less than that of the crustal signal itself[12]. Up to degree 13, however, the Oersted–Magsat spectrum is well above the level (dotted line) defined by both that flat section and the crustal spectrum (the contribution of which is believed to be weaker at low degrees than at high degrees[2]). It is also well above the error level. It thus cannot be attributed to noise or a crustal source. By contrast, it can be explained by core surface flows, as is illustrated by the spectrum of the misfit between the predicted and the observed Oersted minus Magsat field difference. This misfit is at a level comparable to that of the errors in the models and of crustal contributions, but relaxed at the largest degrees to account for 'truncation errors'[17]. For reference, the spectrum of the less-resolved field variations[5] between 1970 and 1990 is also shown.